J. Phys. B: At. Mol. Opt. Phys. **41** (2008) 125701 (10pp) doi:10.1088/0953-4075/41/12/125701

Excitations to the electronic continuum of $^3HeT^+$ in investigations of T_2 β-decay experiments

Natasha Doss and Jonathan Tennyson

Department of Physics and Astronomy, University College London, Gower St, London WC1E 6BT, UK

Received 15 April 2008
Published 6 June 2008
Online at stacks.iop.org/JPhysB/41/125701

Abstract

The final-state probability distribution for excitations to the electronic continuum of $^3HeT^+$ resulting from the β-decay of T_2 is calculated. The R-matrix method is used to obtain a geometry dependant treatment of the resonance states of $^3HeT^+$ allowing for nuclear motion effects of these states to be accounted for explicitly in the determination of the final-state distribution. A discretized distribution for the background continuum is used to obtain this part of the decay probability. When combined with previous studies of other energy ranges, 99.94% of the decay probability is recovered, a significant improvement on previous results.

(Some figures in this article are in colour only in the electronic version)

1. Introduction

The determination of the rest masses of neutrinos is one of the most intriguing yet controversial topics in particle physics today. The existence of a nonzero neutrino mass would have fundamental implications in many areas including cosmology and astrophysics. Experimental investigations of neutrino oscillations have provided compelling evidence for nonzero masses (Fukuda *et al* 1998) and information on the differences in the squared masses of the three neutrino flavours; however, these experiments are insensitive to the absolute masses. Searches for the absolute mass from investigations of neutrinoless double beta decays and cosmological constraints have provided upper limits for the electron neutrino mass, $m_{ee} < 0.7$–2.8 eV$/c^2$ (Arnold *et al* 2005), and the sum of all three neutrino masses, $\sum m_\nu < 0.17$ eV$/c^2$ (Seljak *et al* 2006), respectively. Yet the most direct measurements, and the motivation for this work, are the kinematical measurements from the molecular tritium β-decay experiments, where the electron neutrino mass is obtained by analysing distortions in the electron energy spectrum close to the endpoint. The most recent of these experiments were performed at Mainz and Troitsk from 1994–2001 which reported upper limits of $m_{\bar{\nu}_e} < 2.3$ eV$/c^2$ (Kraus *et al* 2005) and $m_{\bar{\nu}_e} < 2.05$ eV$/c^2$ (Lobashev 2003), respectively. The forthcoming KATRIN (Karlsruhe Tritium Neutrino) experiment (Osipowicz *et al* 2001, Thümmler *et al* 2002) anticipates a sensitivity of the neutrino mass of <0.2 eV (90% C.L.) a factor of ten higher sensitivity compared to Mainz and Troitsk.

In order to determine the neutrino mass from these experiments it is essential to know accurately the distribution of energy released in excitation of the daughter molecule, $^3HeT^+$, produced in the decay. In a previous work by us (Doss *et al* 2006) the calculation of the probability distribution for excitations to the electronic bound states was presented. In this paper, we report our calculation of the final-state distribution to the electronic continuum of $^3HeT^+$.

The electronic continuum of $^3HeT^+$ consists of the background singly excited molecular continuum together with contributions from Feshbach resonances. It has been shown that these resonances track strongly repulsive states of $^3HeT^{2+}$ and therefore have a very strong dependence on the internuclear separation (Tennyson 1998). This means that for an accurate calculation of the final-state distribution of the electronic continuum, the nuclear motion effects must be considered as each resonance will effect a wider range of energies than its (generally) narrow width suggests (Tennyson 1998).

In calculations of the final-state distribution to date, the part associated with the electronic continuum is the least accurately determined. Early works using the stabilization method (Kołos *et al* 1986, Szalewicz *et al* 1987, Froelich *et al* 1987) and the complex scaling method (Froelich *et al* 1993) were limited by the number of resonances obtained

and did not take into account their variation as a function of the internuclear separation, R. The R dependence was later considered explicitly by Saenz and Froelich (1997) by use of the reflection approximation. However, the previous distributions had some missing probability. In the most recent calculation the missing probability, 0.17%, was associated with belonging to the electronic continuum part (Saenz *et al* 2000).

Here we present the calculation of the final-state distribution of the electronic continuum, using a different method to the previous works mentioned above. The R-matrix method has been used to perform a geometry dependant calculation of the $^1\Sigma^+$ total symmetry resonance states of $^3HeT^+$ (as this is the relevant symmetry for T_2 β-decay (Fackler *et al* 1985)). The positions and widths of resonances converging to the first eight excited states of $^3HeT^{2+}$ have been obtained. By performing a similar R-matrix calculation for T_2, the wavefunction for the electronic ground state of T_2 was obtained, and overlap integrals between nine resonance states and the ground state of T_2 were calculated. Probability density distributions for each resonance were then obtained. A discrete probability distribution for the background continuum and remaining resonances has also been determined for $R = 1.4\ a_0$, the equilibrium geometry of $^3HeT^+$.

2. *R*-matrix calculation of the resonance states of $^3HeT^+$

Tennyson (1998) performed a calculation of the resonant states of $^3HeT^+$ converging to the first three excited states of $^3HeT^{2+}$ as a function of internuclear separation, using the UK molecular R-matrix programs (Gillan *et al* 1995). The same method and programs have been used here to perform an improved calculation of the continuum states.

2.1. Method

The R-matrix method is based on the division of configuration space into two regions by a spherical boundary of radius a centred on the centre of mass of the target molecule. a is chosen such that the entire electronic charge distribution of the molecule is contained within the sphere, hence the contributions that dominate the Hamiltonian differ in the two regions.

In the inner region, $r < a$ (where r is the radial coordinate of the scattered electron), the scattered electron lies within the molecular charge cloud and therefore short-range interactions such as electron exchange and correlation must be taken into account. The target molecule and scattering electron complex behaves similarly to a bound state, and so rigorous quantum chemistry methods can be used to obtain the wavefunctions. The inner region scattering energy-independent eigenfunctions of the target molecule plus scattering electron system are represented by a close-coupling expansion,

$$\psi_k^{N+1} = \mathcal{A} \sum_I \psi_I^N(\mathbf{X}_1, \ldots, \mathbf{X}_N) \sum_j \bar{\xi}_j(\mathbf{X}_{N+1}) a_{Ijk} + \sum_m \chi_m(\mathbf{X}_1, \ldots, \mathbf{X}_N, \mathbf{X}_{N+1}) b_{mk}, \quad (1)$$

where $\mathcal{A}$ is the anti-symmetrization operator, ψ_I^N are the target molecular wavefunctions, N is the number of target electrons, $\mathbf{X}_n = (\mathbf{r}_n, \sigma_n)$ where $\mathbf{r}_n$ is the spatial coordinate and σ_n is the spin state of the nth electron, $\bar{\xi}_j$ is a continuum molecular orbital spin-coupled with the scattering electron and a_{Ijk} and b_{mk} are variational coefficients.

The first-term summation runs over configuration interaction target states. It accounts for one electron in a continuum state with the remaining electrons in a target state, known as a 'target + continuum' configuration. The second-term summation runs over configurations χ_m in which all the electrons are placed in target molecular orbitals and are known as L^2 functions. These functions account for polarization and correlation effects. The coefficients a_{Ijk} and b_{mk} are found through diagonalization of the Hamiltonian matrix in the inner region. These energy-independent eigenfunctions have associated energies, E_k, called 'R-matrix poles'.

The full energy-dependant scattering wavefunction in the inner region is a linear combination of the energy-independent eigenfunctions,

$$\Psi_E = \sum_k A_{Ek} \psi_k, \quad (2)$$

with the coefficients A_{Ek} found by matching with the computed outer region functions at the boundary using the R-matrix. The R-matrix on the boundary is determined from the solutions of the Hamiltonian matrix. The R-matrix contains a complete description of the collision problem in the inner region for the energy range defined by the choice of target states and continuum orbitals, and provides the boundary conditions necessary to match the inner and outer region wavefunctions, and solve the problem in the outer region.

In the outer region, $r > a$, exchange and correlation become negligible, and the electron moves in the long-range multi-pole potential of the target and a single-centre expansion of the wavefunction can be used.

For more detailed discussion on the R-matrix approach to electron–molecule scattering see Burke and Berrington (1993).

Calculations on the resonance states of $^3HeT^+$ were performed using the UK molecular R-matrix programs for 21 internuclear separations in the range $R = 1.0$–$2.0\ a_0$, in steps of $0.05\ a_0$.

2.2. Target calculation

The quality of the calculation depends heavily on the quality of the target and hence on the basis set used to represent it. In this calculation a basis set of Slater-type orbitals (STOs) was used. The criteria determining the choice of the STOs are that the basis be small enough to be manageable but flexible enough to be able to represent the target sufficiently at all the internuclear separations used. In this work the basis set used by Tennyson (1998) was taken as a starting point. Tennyson used 3s, 2p and 1d Slater-type orbitals on each atom, where the exponents of each orbital were optimized for the four lowest target states at the equilibrium geometry $R = 1.4\ a_0$ by comparison with exact energies computed using the code of Power (1973). The basis set of Tennyson was adjusted in order to improve the energies of the existing target states and to include higher energy target

Table 1. Slater-type basis set for $^3HeT^{2+}$.

T				He			
n	l	m	ζ	n	l	m	ζ
1	0	0	3.5	1	0	0	7.0
1	0	0	1.741 22	1	0	0	4.058 13
2	0	0	0.941 22	2	0	0	3.126 75
				3	0	0	1.520
2	1	0	1.292 41	2	1	0	1.4109
3	1	0	1.934 96	3	1	0	6.36
3	2	0	1.2	3	2	0	1.25
2	1	1	1.5	2	1	1	2.4
3	1	1	0.8	3	1	1	1.6
3	2	1	1.0	3	2	1	1.25
3	2	2	1.75	3	2	2	1.25

states with reasonable accuracy. For each atom, one compact orbital and one diffuse orbital were added to the basis set. To combat linear dependency problems the exponents were adjusted one at a time until the problem could be eliminated but at the same time trying to retain as much as possible reasonable energies for the target states. The exponents were adjusted by considering their effect at three geometries, $R = 1.0$, 1.4 and 2.0 a_0. To remove the linear dependency entirely the extra diffuse hydrogen orbital added to the set had to be dropped. The final basis set used in this work is given in table 1. The target energy levels calculated using this basis set, as a function of internuclear separation, are given in table 2.

2.3. Scattering calculation

To represent the continuum, numerical functions were obtained by solving for a Coulomb potential $V = -2/r$ (in au) inside the R-matrix sphere using an $l \leqslant 7$ partial wave expansion. A total of 162 orbitals consisting of 64σ, 54π and 44δ orbitals were obtained. Using Lagrange orthogonalization (Tennyson *et al* 1987), 2σ and 1π continuum orbitals were removed from the basis in order to alleviate linear dependence problems. The remaining continuum orbitals were then Schmidt orthogonalized to the entire set of target functions. Using an R-matrix sphere of radius 10 a_0, scattering calculations were performed including all nine of the target states given in table 2. As the target molecule $^3HeT^{2+}$ has just the one electron, it was possible to include all the symmetry allowed L^2 configurations to account for correlation and polarization effects, without the risk of over-correlation of the system.

In the outer region the R-matrices were propagated to 50 a_0 and the K-matrices obtained.

2.4. Resonances

At each internuclear separation, R, resonances converging to the eight excited target states of HeT^{2+} were detected and their positions and widths determined by fitting the associated eigenphase sum to a Breit–Wigner profile. For each resonance, the fit was performed for 20 energy points. The quality of a fit can be defined by the goodness factor gf, which analyses the sum of the residues,

$$gf = -\log_{10}\left|\sum_{i=1}^{20}\eta_{\rm fit}(E_i) - \eta_{\rm calc}(E_i)\right|, \qquad (3)$$

where η is the eigenphase sum. Fits with $gf \geqslant 4$ give reliable results and those with $gf \leqslant 0$ give unreliable results. For intermediate values of gf the positions are reliable but the widths are often too large (Tennyson 1998). Hence gf values give us some idea of the error in the calculated positions and widths which result from the fact that the resonances are not calculated directly, but through a fit procedure.

Resonance curves have been obtained by correlating the resonances detected at different geometries using quantum defect analysis (Seaton 1983). A Rydberg series of resonance

Table 2. Computed energy levels of $^3HeT^{2+}$, in E_h, as a function of the internuclear separation R, in a_0.

R	1sσ	2pσ	2pπ	2sσ	3pσ	3dσ	3dπ	3dδ	3pπ
1.00	−1.031 84	0.664 21	0.974 21	1.092 26	1.487 32	1.497 23	1.499 39	1.517 29	1.535 36
1.05	−1.082 96	0.558 41	0.885 81	1.005 32	1.388 26	1.400 65	1.404 03	1.423 33	1.442 08
1.10	−1.128 11	0.462 46	0.806 05	0.926 80	1.298 22	1.312 71	1.317 36	1.338 07	1.357 49
1.15	−1.168 24	0.375 29	0.733 81	0.855 58	1.216 10	1.232 23	1.238 27	1.260 38	1.280 45
1.20	−1.204 14	0.295 98	0.668 13	0.790 74	1.140 99	1.158 27	1.165 82	1.189 32	1.210 04
1.25	−1.236 46	0.223 73	0.608 20	0.731 49	1.072 09	1.090 02	1.099 22	1.124 09	1.145 46
1.30	−1.265 73	0.157 86	0.553 37	0.677 17	1.008 74	1.026 79	1.037 81	1.064 03	1.086 07
1.35	−1.292 38	0.097 76	0.503 04	0.627 23	0.950 35	0.968 00	0.981 01	1.008 57	1.031 29
1.40	−1.316 77	0.042 90	0.456 73	0.581 18	0.896 43	0.913 16	0.928 34	0.957 21	0.980 65
1.45	−1.339 22	−0.007 20	0.414 01	0.538 61	0.846 53	0.861 83	0.879 37	0.909 54	0.933 74
1.50	−1.359 98	−0.052 96	0.374 52	0.499 17	0.800 28	0.813 65	0.833 73	0.865 19	0.890 21
1.55	−1.379 26	−0.094 76	0.337 93	0.462 53	0.757 35	0.768 29	0.791 11	0.823 84	0.849 74
1.60	−1.397 23	−0.132 95	0.303 96	0.428 43	0.717 42	0.725 49	0.751 23	0.785 21	0.812 09
1.65	−1.414 05	−0.167 85	0.272 37	0.396 63	0.680 22	0.685 03	0.713 84	0.749 05	0.777 01
1.70	−1.429 85	−0.199 73	0.242 94	0.366 92	0.645 17	0.647 03	0.678 71	0.715 16	0.744 30
1.75	−1.444 74	−0.228 85	0.215 47	0.339 10	0.609 65	0.613 73	0.645 65	0.683 33	0.713 78
1.80	−1.458 80	−0.255 45	0.189 80	0.313 02	0.574 92	0.583 53	0.614 48	0.653 40	0.685 31
1.85	−1.472 11	−0.279 75	0.165 77	0.288 52	0.541 69	0.555 39	0.585 05	0.625 21	0.658 73
1.90	−1.484 76	−0.301 94	0.143 24	0.265 47	0.509 89	0.529 12	0.557 22	0.598 64	0.633 92
1.95	−1.496 78	−0.322 20	0.122 09	0.243 75	0.479 41	0.504 57	0.530 85	0.573 55	0.610 77
2.00	−1.508 24	−0.340 69	0.102 21	0.223 26	0.450 16	0.481 63	0.505 84	0.549 83	0.589 18

states converges to each electronic state of $^3HeT^{2+}$. The quantum defect can be used to parameterize a Rydberg series of states below a threshold. This has proved to be the most reliable method of interpolating resonance parameters over a grid of geometries (Tennyson 1988).

In each series there is one member for each (n, l) combination with $n > l$. There are therefore an infinite number of increasingly narrow resonances in each series.

The complex quantum defect μ_{nl} is given by

$$\mu_{nl} = \alpha_{nl} + i\beta_{nl}. \tag{4}$$

From the position determined by the fit the effective quantum number n^* of the resonance is determined using the relation

$$E_{\text{target}} - E_{\text{res}} = \frac{R_\infty Z^2}{(n^*)^2}, \tag{5}$$

where $E_{\text{res}}(R)$ and $E_{\text{target}}(R)$ are the energies at R of the resonance and the relevant 'parent' target state threshold, respectively, R_∞ is the Rydberg constant and Z is the residual charge. The effective quantum number n^* is related to the real part of the complex quantum defect, α_{nl}, by

$$n^* = n - \alpha_{nl}, \tag{6}$$

where α_{nl} (and hence n^*) varies gently and smoothly as a function of internuclear separation. Resonances were matched at different geometries by matching their effective quantum numbers. α_{nl} has a very weak dependence on n but depends strongly on l. In general, α_{nl} decreases rapidly as l increases. It is therefore generally easier to match n^* for the low-l states than for the high-l states because at high-l the quantum defects are close to zero. Within a series of resonances converging to a particular target state, it is also possible to identify separate series of resonances with increasing n but the same l as the quantum defects will be the same for these resonances and so the effective quantum numbers will differ by a whole number.

A total of 40 resonance curves converging to the first three excited states of $^3HeT^{2+}$ were obtained. These curves together with the $^3HeT^{2+}$ target states are shown in figure 1. As shall be discussed in the following section, it was not possible to account for the nuclear motion effects of all 40 resonances when determining the final-state probability distribution. The positions, widths, goodness factors and effective quantum numbers of the nine resonance states for which nuclear motion effect was taken into account are given in table 3. The assignments of the resonance states comes from the quantum defect analysis, but they should not be regarded as definitive. Resonance energies for the first five resonances are in agreement with those given by Saenz (2003) to within 0.005 E_h for all geometries except for $R = 1.0\,a_0$ for the $2p\sigma\,3p\sigma$ resonance.

The $n = 3$ electronic states of $^3HeT^{2+}$ lie very close together in energy (see table 2). The resonances detected above the $2s\sigma$ and below the $3p\sigma$ state are not all related to the series converging to $3p\sigma$, but include contributions from resonances converging to the other $n = 3$ states. These resonances lie very close together and make the interpolation of the resonances as a function of R very difficult. Therefore resonance curves for the resonances detected between the $2s\sigma$ and $3p\sigma$ states were not determined. The resonances detected above $3p\sigma$ have

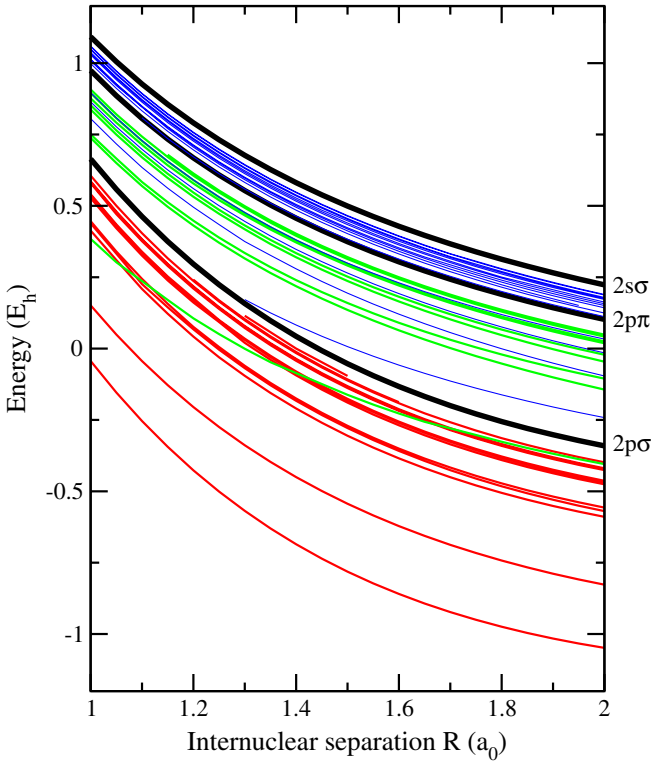

Figure 1. $^3HeT^+$ resonance curves and $^3HeT^{2+}$ target potentials as a function of internuclear separation R. Resonances converging to the $2p\sigma$, $2p\pi$ and 2s target states are drawn in red, green and blue, respectively.

negative goodness factors implying that the fit is poor, hence these resonances were ignored.

In principle there are an infinite number of resonances associated with each target state for each n and each l. There is in fact a double infinity, as for each l there is an infinite number of n, and there are an infinite number of l. However in practise the number of resonances determined is limited by the choice of partial waves, which in this calculation is states with $l \leqslant 7$. Hence we have assumed that states with $l > 7$ have quantum defects very close to zero.

3. Final-state distribution results

The contribution to the final-state probability distribution of the electronic continuum from the resonance states and the background continuum were calculated separately. Transitions involving the β-decay of T_2 molecules in the ground rovibrational level of the $n = 1$ electronic state were considered.

3.1. Probability distribution of the resonance states

The probability distribution involving transitions to the nuclear motion continuum of the electronically bound states of $^3HeT^+$ is given by Jeziorski *et al* (1985),

$$P_{nJ}(E) = (2J+1) \times \left| \int_0^\infty S_n(R)\, j_J(KR)\, f_{nJ}^{^3HeT^+}(R|E)\, f_{100}^{T_2}(R)\, dR \right|^2, \tag{7}$$

where $P_{nJ}(E)$ is the probability per unit energy that the $^3HeT^+$ molecule dissociates via the nth electronic state and

Table 3. Positions $E_{\rm res}$ and widths Γ for $^1\Sigma^+$ resonance states of ^{3}HeT$^+$, as a function of internuclear separation R. Also given are assignments, effective quantum numbers n^* and goodness factors gf.

R (a_0)	$E_{\rm res}$ (E_h)	Γ (E_h)	n^*	gf	$E_{\rm res}$ (E_h)	Γ (E_h)	n^*	gf
		$2p\sigma^2$				$2p\sigma 3s$		
1.00	−0.043 49	0.026 07	1.681 09	9	0.151 36	0.017 04	1.974 79	8
1.05	−0.153 85	0.026 44	1.675 71	7	0.049 10	0.017 56	1.981 65	7
1.10	−0.253 79	0.026 55	1.671 00	6	−0.043 66	0.017 93	1.987 87	7
1.15	−0.344 01	0.026 56	1.667 47	6	−0.128 17	0.018 30	1.993 12	7
1.20	−0.426 47	0.026 45	1.663 84	6	−0.204 90	0.018 19	1.998 25	7
1.25	−0.501 01	0.026 29	1.661 21	6	−0.274 83	0.018 02	2.002 90	8
1.30	−0.568 64	0.026 00	1.659 20	7	−0.338 63	0.017 80	2.007 06	8
1.35	−0.629 97	0.025 55	1.657 79	9	−0.396 92	0.017 53	2.010 74	7
1.40	−0.685 57	0.024 93	1.656 96	8	−0.450 22	0.017 22	2.013 92	7
1.45	−0.735 90	0.024 12	1.656 69	7	−0.498 98	0.016 85	2.016 65	7
1.50	−0.781 42	0.023 16	1.656 96	7	−0.543 61	0.016 41	2.018 97	7
1.55	−0.822 53	0.022 09	1.657 74	8	−0.584 46	0.015 93	2.020 93	7
1.60	−0.859 64	0.020 92	1.658 99	8	−0.621 86	0.015 40	2.022 55	8
1.65	−0.893 07	0.019 69	1.660 65	9	−0.656 11	0.014 86	2.023 90	8
1.70	−0.923 17	0.018 43	1.662 70	9	−0.687 47	0.014 30	2.024 98	9
1.75	−0.950 22	0.017 18	1.665 08	8	−0.716 18	0.013 75	2.025 84	10
1.80	−0.974 50	0.015 94	1.667 77	8	−0.742 46	0.013 20	2.026 50	10
1.85	−0.996 25	0.014 75	1.670 73	8	−0.766 53	0.012 68	2.026 98	9
1.90	−1.015 72	0.013 58	1.673 92	8	−0.788 56	0.012 17	2.027 30	9
1.95	−1.033 09	0.012 47	1.677 30	8	−0.808 73	0.011 69	2.027 49	8
2.00	−1.048 57	0.011 40	1.680 87	8	−0.827 19	0.011 22	2.027 56	8
		$2p\sigma 3p\sigma$				$2p\sigma 3d\sigma$		
1.00	0.413 55	0.003 98	2.824 71	6	0.438 63	0.001 48	2.977 59	6
1.05	0.310 31	0.004 39	2.839 27	4	0.332 68	0.002 01	2.976 65	5
1.10	0.208 80	0.005 35	2.807 95	5	0.225 98	0.005 80	2.908 17	6
1.15	0.122 08	0.004 77	2.810 44	6	0.144 66	0.004 15	2.944 77	5
1.20	0.041 96	0.004 61	2.805 97	6	0.067 44	0.003 14	2.958 23	4
1.25	−0.030 51	0.004 41	2.804 74	6	−0.003 90	0.002 68	2.964 14	5
1.30	−0.095 47	0.004 29	2.809 82	6	−0.068 72	0.002 55	2.971 06	5
1.35	−0.155 36	0.004 10	2.810 96	7	−0.128 31	0.002 27	2.974 41	5
1.40	−0.210 03	0.003 90	2.812 05	7	−0.182 85	0.002 03	2.976 52	5
1.45	−0.259 85	0.003 69	2.813 57	7	−0.232 76	0.001 82	2.977 71	5
1.50	−0.305 29	0.003 47	2.815 33	7	−0.278 46	0.001 68	2.978 13	5
1.55	−0.346 75	0.003 24	2.817 24	7	−0.320 31	0.001 57	2.977 82	5
1.60	−0.384 58	0.003 01	2.819 28	7	−0.358 63	0.001 51	2.976 93	5
1.65	−0.419 09	0.002 77	2.821 45	7	−0.393 72	0.001 49	2.975 62	5
1.70	−0.450 57	0.002 54	2.823 65	7	−0.425 87	0.001 49	2.973 87	6
1.75	−0.479 33	0.002 31	2.825 72	8	−0.455 33	0.001 52	2.971 67	6
1.80	−0.505 55	0.002 08	2.827 85	8	−0.482 30	0.001 55	2.969 25	6
1.85	−0.529 49	0.001 88	2.829 89	8	−0.507 01	0.001 61	2.966 57	6
1.90	−0.551 34	0.001 67	2.831 80	8	−0.529 64	0.001 66	2.963 71	6
1.95	−0.571 30	0.001 48	2.833 53	8	−0.550 35	0.001 71	2.960 71	6
2.00	−0.589 54	0.001 30	2.834 95	8	−0.569 33	0.001 76	2.957 56	6
		$2p\sigma 4s$				$2p\sigma 4d\sigma$		
1.00	0.446 46	0.002 08	3.030 65	5	0.536 45	0.000 90	3.956 64	5
1.05	0.340 13	0.001 99	3.026 98	5	0.430 68	0.000 95	3.957 07	5
1.10	0.244 20	0.003 94	3.027 09	2	0.335 37	0.000 90	3.966 98	5
1.15	0.157 05	0.002 37	3.027 20	7	0.248 73	0.000 90	3.975 18	5
1.20	0.076 01	0.002 96	3.015 35	5	–	–	–	–
1.25	0.005 44	0.003 26	3.026 91	5	–	–	–	–
1.30	−0.060 25	0.003 46	3.028 14	4	–	–	–	–
1.35	−0.120 29	0.003 70	3.028 61	4	–	–	–	–
1.40	−0.175 04	0.003 90	3.029 37	4	–	–	–	–
1.45	−0.225 02	0.004 07	3.030 16	4	–	–	–	–
1.50	−0.270 65	0.004 14	3.031 07	4	−0.180 91	0.001 92	3.953 57	4
1.55	−0.312 31	0.004 16	3.032 05	4	−0.222 08	0.001 38	3.963 42	4
1.60	−0.350 37	0.004 12	3.032 99	4	−0.260 00	0.001 13	3.967 60	4
1.65	−0.385 11	0.004 05	3.034 05	4	−0.294 80	0.001 01	3.969 06	4
1.70	−0.416 84	0.003 93	3.035 10	5	−0.326 67	0.000 96	3.969 20	4
1.75	−0.445 82	0.003 82	3.036 06	5	−0.355 83	0.000 93	3.968 63	4
1.80	−0.472 28	0.003 67	3.037 07	5	−0.382 52	0.000 95	3.967 34	3
1.85	−0.496 45	0.003 53	3.037 97	5	−0.406 92	0.000 91	3.965 79	4

Table 3. (Continued.)

R (a_0)	$E_{\rm res}$ (E_h)	Γ (E_h)	n^*	gf	$E_{\rm res}$ (E_h)	Γ (E_h)	n^*	gf
1.90	−0.518 50	0.003 37	3.038 94	5	−0.429 23	0.000 94	3.963 86	3
1.95	−0.538 63	0.003 22	3.039 84	6	−0.449 62	0.000 93	3.961 82	4
2.00	−0.556 99	0.003 07	3.040 76	6	−0.468 23	0.000 96	3.959 91	3
		$2p\sigma 5s$				$2p\pi^2$		
1.00	0.540 77	0.000 83	4.025 31	5	0.384 29	0.000 60	1.841 28	6
1.05	0.435 06	0.000 78	4.026 83	5	0.302 43	0.009 24	1.851 57	2
1.10	0.339 20	0.000 89	4.028 13	5	–	–	–	–
1.15	0.252 55	0.000 94	4.036 62	5	0.170 54	0.005 22	1.884 33	5
1.20	0.176 04	0.001 01	4.083 47	6	0.105 98	0.000 62	1.886 21	5
1.25	0.099 98	0.000 87	4.020 17	5	0.050 85	0.005 93	1.894 30	4
1.30	0.034 83	0.001 44	4.032 02	4	−0.000 57	0.006 16	1.900 14	6
1.35	−0.025 22	0.001 68	4.032 84	2	−0.047 78	0.006 31	1.905 51	3
1.40	−0.080 45	0.001 48	4.026 71	2	–	–	–	–
1.45	−0.130 34	0.001 58	4.030 13	5	−0.124 08	0.003 14	1.927 91	4
1.50	−0.176 01	0.001 67	4.031 57	4	−0.162 00	0.004 36	1.930 74	5
1.55	−0.217 74	0.001 70	4.032 75	4	−0.196 10	0.004 72	1.935 23	8
1.60	−0.255 88	0.001 71	4.033 56	4	−0.227 54	0.004 70	1.939 83	5
1.65	−0.290 70	0.001 69	4.034 75	4	−0.256 62	0.004 99	1.944 42	2
1.70	−0.322 51	0.001 66	4.035 98	4	–	–	–	–
1.75	−0.351 57	0.001 61	4.037 04	4	−0.302 75	0.002 68	1.964 52	4
1.80	−0.378 10	0.001 56	4.038 23	5	−0.326 51	0.003 34	1.968 16	5
1.85	−0.402 32	0.001 49	4.039 41	5	−0.348 28	0.003 56	1.972 49	6
1.90	−0.424 44	0.001 43	4.040 58	5	−0.368 46	0.003 56	1.977 01	6
1.95	−0.444 63	0.001 37	4.041 73	5	−0.387 23	0.003 45	1.981 62	5
2.00	−0.463 05	0.001 31	4.042 84	5	−0.404 72	0.003 28	1.986 29	4
		2s3s						
1.00	–	–	–	–				
1.05	–	–	–	–				
1.10	–	–	–	–				
1.15	–	–	–	–				
1.20	–	–	–	–				
1.25	–	–	–	–				
1.30	0.171 74	0.006 17	1.989 23	8				
1.35	0.125 23	0.006 03	1.996 02	8				
1.40	0.082 52	0.005 90	2.002 69	8				
1.45	0.043 20	0.005 76	2.009 24	9				
1.50	0.006 92	0.005 62	2.015 69	9				
1.55	−0.026 65	0.005 50	2.022 00	9				
1.60	−0.057 77	0.005 39	2.028 18	9				
1.65	−0.086 67	0.005 28	2.034 26	9				
1.70	−0.113 57	0.005 19	2.040 21	9				
1.75	−0.138 64	0.005 11	2.046 07	9				
1.80	−0.162 05	0.005 04	2.051 82	9				
1.85	−0.183 94	0.004 97	2.057 48	9				
1.90	−0.204 45	0.004 91	2.063 03	9				
1.95	−0.223 68	0.004 87	2.068 51	9				
2.00	−0.241 75	0.004 83	2.073 88	9				

that the dissociation products are in a state with energy E and angular momentum J, $j_J(KR)$ is the spherical Bessel function, $f_{100}^{\rm T_2}(R)$ is the radial vibrational wave function of the $n = 1$, $v = 0$, $J = 0$ state of T_2 and $f_{nJ}^{^3{\rm HeT}^+}(R|E)$ is the energy normalized radial function of the continuous spectrum. $S_n(R)$ is the overlap integral providing the R-dependent probability amplitude of transition to the nth electronic state of the daughter system given by

$$S_n(R) = \int \psi_n^{^3{\rm HeT}^+ *}(r_1, r_2; R)\psi_1^{\rm T_2}(r_1, r_2; R)\,{\rm d}r_1\,{\rm d}r_2, \quad (8)$$

where $\psi_n^c(r_1, r_2; R)$ are the clamped-nuclei electronic wavefunctions for the initial ($c = T_2$) and final ($c = {}^3HeT^+$) state.

This equation is also valid for calculating the probability density distribution of the resonance states if they are considered as quasibound states embedded in the continuum and are decoupled from the background continuum. The label n in equations (7) and (8) now refers to the combined configuration of the two electrons. By using this equation, the R dependence of the resonance is taken into account explicitly. $S_n(R)$ is now the overlap integral of the resonance state and the electronic state of the daughter system.

In order to determine $S_n(R)$ several assumptions were made. The first key assumption is that the wavefunction describing the ground electronic state of T_2, with energy $E_1^{\rm T_2}$, is entirely localized inside the R-matrix sphere. Therefore in

equation (2) the coefficient A_{Ek} at $E \simeq E_1^{T_2}$ becomes the Dirac delta function, $\delta\left(E - E_1^{T_2}\right)$, and so the wavefunction for the T_2 ground state is given by the eigenfunction $\psi_1^{T_2}$ which has an associated R-matrix pole $E_k \simeq E_1^{T_2}$. This is a valid assumption for the compact ground electronic state of T_2 which is the only state considered here. By making this assumption the total wavefunction describing the $^3HeT^+$ system in the outer region can be ignored as the overlap of this wavefunction with the T_2 wavefunction will be zero.

The next assumption made was that the wavefunction describing the resonance is also totally localized inside the R-matrix box. This is a reasonable assumption for the low-lying resonances but becomes worse for higher lying resonances. The coefficient A_{Ek} at $E \simeq E_{res}$ becomes the Dirac delta function, and so the wavefunction for the resonance is given by the eigenfunction $\psi_k^{^3HeT^+}$ with an associated R-matrix pole $E_k \simeq E_{res}$.

The eigenfunction describing the resonance state n is given by (cf equation (1)),

$$\psi_n^{^3HeT^+}(r_1, r_2; R) = \sum_l c_l(R)\phi_l^{CSF}(r_1, r_2), \tag{9}$$

where ϕ_l^{CSF} are configuration state functions normalized over the inner region, which include the contribution from both the 'target + continuum' functions and L^2 functions. Similarly, the eigenfunction describing the T_2 ground state is given by

$$\psi_1^{T_2}(r_1, r_2; R) = \sum_m d_m(R)\varphi_m^{CSF}(r_1, r_2), \tag{10}$$

and the overlap integral is then

$$S_n(R) = \int \sum_l c_l^*(R)\phi_l^{CSF*}(r_1, r_2) \times \sum_m d_m(R)\varphi_m^{CSF}(r_1, r_2)\, dr_1\, dr_2. \tag{11}$$

If $\psi_n^{^3HeT^+}$ and $\psi_1^{T_2}$ are expanded in the same basis, i.e. ϕ_l^{CSF} and φ_m^{CSF} are identical, then $S_n(R)$ reduces to

$$\begin{aligned} S_n(R) &= \sum_l c_l^*(R) \sum_m d_m(R) \\ &\quad \times \int \phi_l^{CSF*}(r_1, r_2)\varphi_m^{CSF}(r_1, r_2)\, dr_1\, dr_2 \\ &= \delta_{lm} \sum_l c_l^*(R) d_l(R), \end{aligned} \tag{12}$$

which is a straightforward vector product.

The wavefunction for T_2 was obtained by performing an e–T_2^+ scattering calculation. To obtain $\psi_1^{T_2}$ in the same basis as $\psi_n^{^3HeT^+}$ the scattering calculation was performed using the same target molecular orbitals and continuum orbitals as in the e–$^3HeT^{2+}$ calculation, for the same geometries. At each R, the first R-matrix pole corresponds to the ground state of T_2. The eigenfunction associated to that pole was therefore selected to represent the state at that R. The R-matrix poles obtained for the T_2 ground state in this calculation are given in table 4. The poles are in good agreement with the T_2 potential from (Wolniewicz 1993), with differences less than 0.0025 E_h, which confirms the validity of the assumption made on the entire localization of the T_2 ground-state wavefunction inside the R-matrix sphere.

Table 4. Energies of the T_2 ground state, in E_h, as a function of the internuclear separation R, in a_0, obtained in the R-matrix calculation. Also given is the T_2 potential from Wolniewicz (1993) (column 3).

R	R-matrix	Wolniewicz (1993)
1.00	−1.121 904 077	−1.124 350 006
1.05	−1.136 284 136	–
1.10	−1.147 507 149	−1.149 874 337
1.15	−1.156 087 015	–
1.20	−1.162 466 567	−1.164 758 239
1.25	−1.166 992 423	–
1.30	−1.169 962 863	−1.172 175 518
1.35	−1.171 621 233	−1.173 794 540
1.40	−1.172 174 258	−1.174 308 820
1.45	−1.171 796 390	−1.173 892 312
1.50	−1.170 632 358	−1.172 692 313
1.55	−1.168 819 496	–
1.60	−1.166 448 621	−1.168 424 160
1.65	−1.163 614 991	–
1.70	−1.160 400 060	−1.162 302 522
1.75	−1.156 870 805	–
1.80	−1.153 085 747	−1.154 915 030
1.85	−1.149 094 483	–
1.90	−1.144 941 649	–
1.95	−1.140 664 067	–
2.00	−1.136 295 566	−1.137 982 819

The electronic wavefunctions for the resonance states can be extracted from the R-matrix calculation, however it is more complicated. There are a large number of poles that lie in the energy region corresponding to the electronic continuum of $^3HeT^+$, whose associated eigenfunctions $\psi_k^{^3HeT^+}$ describe the resonance states and the background continuum in a discrete form. To identify which eigenfunction represents a particular resonance two methods were used simultaneously. First, as the poles lie close together, the resonances were matched to poles by their effective quantum number rather than matching by energy. n^* were obtained for all of the poles. Although this proved to be simpler than matching by energy, there were cases where a pair of poles had very similar n^*. Even though the entire localization of the resonance inside the R-matrix sphere is a reasonable assumption for lower lying resonances, it is not exact, hence the resonance energy will not match a pole exactly but be very close to it. This means that the pole with the closest energy may not necessarily be the one describing the resonance.

The second method used was to analyse the overlaps of all the eigenfunctions with the ground state T_2 eigenfunction $\psi_1^{T_2}$. For every eigenfunction ψ_k in the set, the overlap $S_n(R)$ was obtained by using equation (12) for every geometry. It is expected the eigenfunctions describing the resonance states will have larger overlaps than those describing the background continuum. This was found to be true for most of the poles. Using both these methods simultaneously, the poles, eigenfunctions and overlap integrals as a function of R for nine resonance states were determined.

For some of the cases where the pole describing the resonance state lay very close to another pole there was some

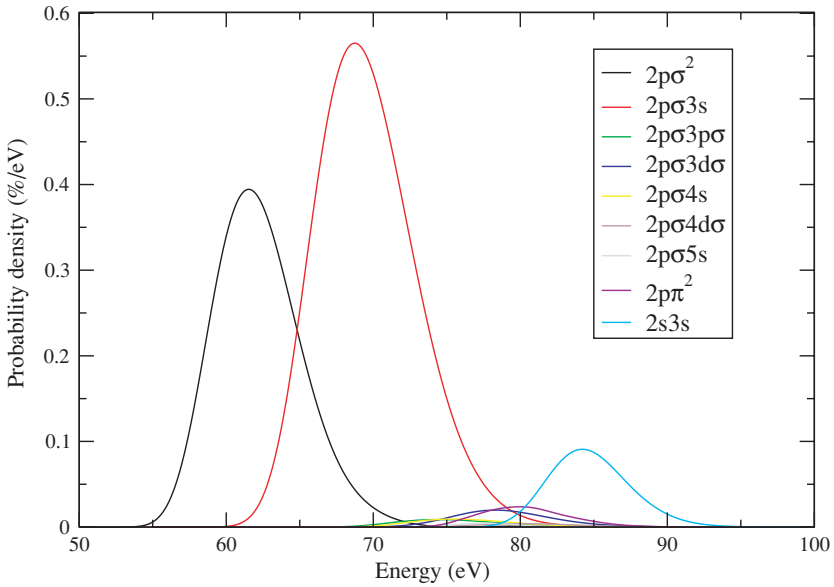

Figure 2. Final-state probability density distribution for nine resonance states of $^3HeT^+$ resulting from the β-decay of a T_2 molecule in the ground rovibrational state of the $n = 1$ electronic state.

Table 5. Overlap integrals $S_n(R)$ between nine resonance states of $^3HeT^+$ with the electronic ground state of T_2.

R	$2p\sigma^2$	$2p\sigma 3s$	$2p\sigma 3p\sigma$	$2p\sigma 3d\sigma$	$2p\sigma 4s$	$2p\sigma 4d\sigma$	$2p\sigma 5s$	$2p\pi^2$	$2s2p\sigma$
1.00	–	–	0.027 16	–	–	–	–	–	–
1.05	–	–	0.026 30	–	0.021 16	–	–	–	–
1.10	–	–	0.026 00	–	0.022 31	–	–	–	–
1.15	–	–	0.025 76	–	0.023 69	–	–	–	–
1.20	0.097 74	0.197 51	0.025 68	0.053 81	0.023 52	–	–	0.050 95	–
1.25	0.112 81	0.201 46	0.024 46	0.051 89	0.023 24	0.021 90	0.010 19	0.048 86	–
1.30	0.120 16	0.205 04	0.023 86	0.049 59	0.023 31	0.020 27	0.009 71	0.044 37	0.080 73
1.35	0.144 83	0.208 41	0.024 37	0.046 59	0.024 94	0.019 10	0.009 47	0.042 72	0.080 37
1.40	0.160 25	0.211 28	0.024 87	0.042 91	0.025 97	0.019 28	0.009 40	0.039 45	0.079 22
1.45	0.177 65	0.216 57	0.026 66	0.037 85	0.027 47	0.019 83	–	0.039 56	0.078 20
1.50	0.191 83	0.222 52	0.028 49	0.032 49	0.029 42	0.014 08	0.022 34	0.039 47	0.077 76
1.55	0.202 21	0.230 58	0.030 20	0.027 56	0.031 43	0.015 60	0.022 65	0.039 26	0.076 19
1.60	0.215 06	0.240 88	0.033 82	–	0.034 32	0.016 00	0.022 20	0.041 56	0.074 41
1.65	0.225 35	0.248 30	–	–	–	0.015 50	0.021 48	0.040 80	0.070 58
1.70	0.233 46	0.255 36	–	–	–	0.016 20	0.018 80	0.039 02	0.069 63
1.75	0.234 84	0.257 01	–	–	–	0.015 32	0.019 19	0.039 09	0.066 69
1.80	0.234 47	0.261 22	–	–	–	0.014 53	0.019 76	0.038 86	0.063 12
1.85	0.235 56	0.265 74	–	–	–	0.012 05	0.021 74	0.042 14	0.060 91
1.90	0.235 20	0.269 92	–	–	–	0.012 18	0.021 96	0.036 44	0.054 55
1.95	0.236 96	0.274 06	–	–	–	0.011 21	0.022 66	0.042 03	0.053 60
2.00	0.237 51	0.279 09	–	–	–	0.012 00	0.024 66	0.033 06	0.046 17

mixing of the overlaps, resulting in a slightly too small or too large value for the overlap of the resonance at that R. To treat this the overlap was smoothed using those at the neighbouring geometries. The smoothed overlaps $S_n(R)$ for the nine resonance states are given in table 5. At some geometries it was not possible to determine the correct pole with sufficient certainty and no overlap was determined. For some of the higher lying resonances which lie very close together, it was not possible to identify the corresponding eigenfunction because of the overlap mixing. For even higher resonances the transition probability to these states is very small and so the overlap integral for the resonances is of the same order as the overlap for the background continuum.

The probability density distribution of each resonance was obtained by using a modified version of the BCONT program by Le Roy (1989) as in Doss *et al* (2006), to calculate the radial functions $f^{T_2}_{100}(R)$ and $f^{^3HeT^+}_{nJ}(R|E)$ and hence the probability density $P_{nJ}(E)$ for the β-decay of a T_2 molecule in the ground rovibrational state of the $n = 1$ electronic state. The probability density distributions of the nine resonance states of $^3HeT^+$ are shown in figure 2. The total probabilities associated with each resonance are given in table 6 together with the probabilities obtained by Froelich *et al* (1993) for the first five resonances. As can be seen from the figure and table, there is a significant contribution from the $2p\pi^2$ and $2s2p\sigma$ which were not present in the calculation of Froelich *et al* (1993).

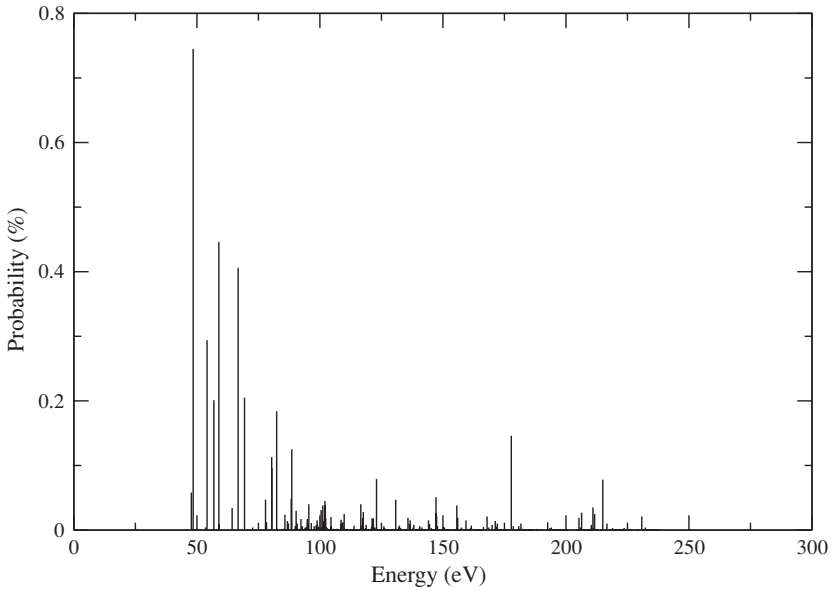

Figure 3. Discrete final-state probability distribution of the background continuum and remaining resonances.

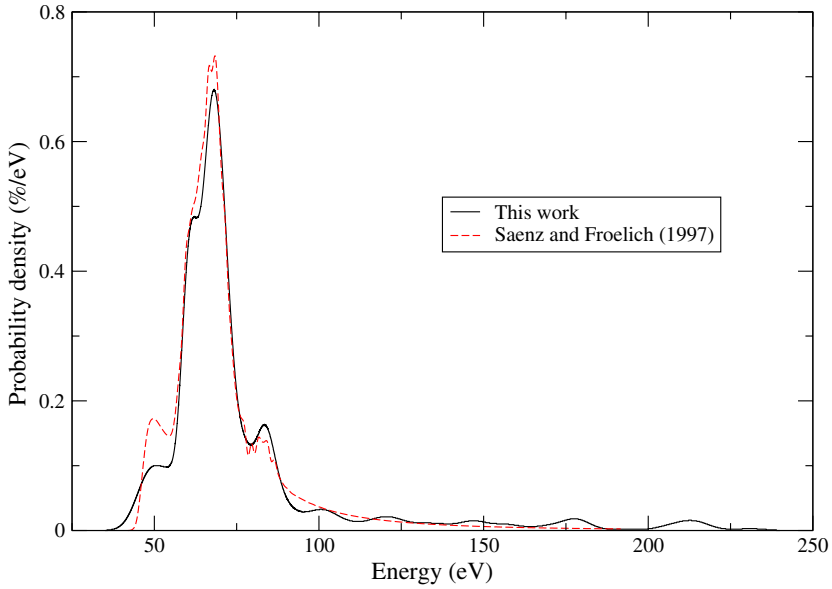

Figure 4. Comparison of the final-state distribution of the electronic continuum of $^3HeT^+$ obtained in this work with the distribution of Saenz and Froelich (1997).

3.2. Probability distribution of the background continuum

The total transition probability P_n from the T_2 ground state to all rovibrational and scattering states associated with the nth electronic state of $^3HeT^+$ is given by Wolniewicz (1965),

$$P_n = \int_0^\infty S_n(R) f_{100}^{T_2}(R)\, dR. \tag{13}$$

If $S_n(R)$ is a slowly varying function of R then

$$P_n \simeq S_n^2(R_e) \int_0^\infty \left[f_{100}^{T_2}(R)\right]^2 dR$$
$$= S_n^2(R_e), \tag{14}$$

where R_e is the equilibrium geometry of the T_2 molecule ($R_e = 1.4\ a_0$). Hence if nuclear motion is not taken into account, the probability to a given state n is simply given by the overlap integral squared.

If the eigenfunctions $\psi_k^{^3HeT^+}$ representing the nine resonance states are removed from the complete set given by the R-matrix calculation, as well as those representing the bound states, the remaining eigenfunctions can be used as a discrete representation of the background continuum and the remaining infinite number of resonances. Equation (14) was used to obtain the discrete probability distribution of the background continuum and the remaining resonances. These results are shown in figure 3.

To obtain a continuous final-state spectrum of the background continuum, a Gaussian was run through the discrete distribution with an energy resolution of 4 eV.

Table 6. Total probabilities, in %, of nine resonance states of $^3HeT^+$. For comparison, the probabilities obtained for the first five resonances of Froelich *et al* (1993) are also given.

Resonance	This work	Froelich *et al* (1993)
$2p\sigma^2$	2.91	2.9
$2p\sigma 3s$	4.74	4.8
$2p\sigma 3p\sigma$	0.08	0.02
$2p\sigma 3d\sigma$	0.16	0.2
$2p\sigma 4s$	0.08	0.3
$2p\sigma 4d\sigma$	0.03	–
$2p\sigma 5s$	0.03	–
$2p\pi^2$	0.17	–
2s3s	0.61	–

3.3. Final distribution

In figure 4, the final-state distribution of the electronic continuum of $^3HeT^+$ obtained in this work up to 240 eV is compared to the distribution of Saenz and Froelich (1997).

The total probability associated with the electronic continuum obtained in this work up to 240 eV is 13.66%. Above 240 eV the total probability from the background continuum and remaining resonances is 0.58%. Summing this probability to the contribution from the electronic bound states calculated by us Doss *et al* (2006) and the contribution from the high lying electronic (Rydberg) states (Jonsell *et al* 1999), the total probability is 99.94%. Thus some of the missing probability, 0.11%, has been recovered in our calculation of the final-state distribution.

4. Conclusions

We have calculated the final-state probability distribution of the electronic continuum of $^3HeT^+$. The *R*-matrix method has been used to perform a geometry dependent treatment of the resonance state of $^3HeT^+$ by considering electron collisions with a $^3HeT^{2+}$ target. Positions and widths of 40 resonance states converging to the first eight excited states of $^3HeT^{2+}$ have been obtained for 21 internuclear separations in the range $R = 1.0$–$2.0\ a_0$. Resonance curves were obtained by correlating the resonances detected at different geometries using quantum defect analysis. The probability distributions for the resonances was obtained, accounting explicitly for the nuclear motion effects. A discrete probability of the background and remaining infinite number of resonances was determined for the $^3HeT^+$ equilibrium geometry, $R = 1.4\ a_0$. We believe that this study resolves the molecular physics issues associated to excitations to the electronic continuum of $^3HeT^+$, and together with our calculation of the bound states, the final-state distribution is determined well enough not to cause systematic errors within the sensitivity of the KATRIN experiment.

Acknowledgments

We would like to thank Svante Jonsell and Alejandro Saenz for helpful discussions.

References

Arnold R *et al* 2005 *Phys. Rev. Lett.* **95** 182302
Burke P G and Berrington K A 1993 *Atomic and Molecular Processes: An R-matrix Approach* (Bristol: Institute of Physics Publishing)
Doss N, Tennyson J, Saenz A and Jonsell S 2006 *Phys. Rev.* C **73** 025502
Fackler O, Jeziorski B, Kołos W, Monkhorst H J and Szalewicz K 1985 *Phys. Rev. Lett.* **55** 1388–91
Froelich P, Jeziorski B, Kołos W, Monkhorst H, Saenz A and Szalewicz K 1993 *Phys. Rev. Lett.* **71** 2871–4
Froelich P, Szalewicz K, Jeziorski B, Kołos W and Monkhorst H J 1987 *J. Phys. B: At. Mol. Phys.* **20** 6173–87
Fukuda Y *et al* 1998 *Phys. Rev. Lett.* **81** 1562–7
Gillan C J, Tennyson J and Burke P G 1995 *Computational Methods for Electron Molecule Collisions* ed W M Huo and F A Gianturco (New York: Plenum)
Jeziorski B, Kołos W, Szalewicz K, Fackler O and Monkhorst H J 1985 *Phys. Rev.* A **32** 2573–83
Jonsell S, Saenz A and Froelich P 1999 *Phys. Rev.* C **60** 034601
Kołos W, Jeziorski B, Monkhorst H J and Szalewicz K 1986 *Int. J. Quantum Chem.* S **19** 421–41
Kraus C *et al* 2005 *Eur. Phys. J.* C **40** 447–68
Le Roy R J 1989 *Comput. Phys. Commun.* **52** 383–95
Lobashev V M 2003 *Nucl. Phys.* A **719** 153–60
Osipowicz A *et al* 2001 *FZKA Scientific Report* 6691 arXiv hep-ex/0109033
Power J D 1973 *Quantum Chem. Program Exch.* **11** 233
Saenz A 2003 *Phys. Rev.* A **67** 033409
Saenz A and Froelich P 1997 *Phys. Rev.* C **56** 2162–84
Saenz A, Jonsell S and Froelich P 2000 *Phys. Rev. Lett.* **84** 242–5
Seaton M J 1983 *Rep. Prog. Phys.* **46** 167–257
Seljak U, Slosar A and McDonald P 2006 *J. Cosmol. Astropart. Phys.* JCAP10(2006)014
Szalewicz K, Fackler O, Jeziorski B, Kołos W and Monkhorst H J 1987 *Phys. Rev.* A **35** 965–79
Tennyson J 1988 *J. Phys. B: At. Mol. Opt. Phys.* **21** 806–15
Tennyson J 1998 *J. Phys. B: At. Mol. Opt. Phys.* **31** L177–85
Tennyson J, Burke P G and Berrington K A 1987 *Comput. Phys. Commun.* **47** 207–12
Thümmler T *et al* 2002 *FZKA Scientific Report* 6752
Wolniewicz L 1965 *J. Chem. Phys.* **43** 1087–91
Wolniewicz L 1993 *J. Chem. Phys.* **99** 1851–68